Controlling aggregate thin film surface morphology for improved light trapping using a patterned deposition rate profile

Xinyu Zhang [a], Jianqiao Huang [a], Gangshi Hu [a], Gerassimos Orkoulas [a], Panagiotis D. Christofides [a,b,*]

[a] Department of Chemical and Biomolecular Engineering, University of California, Los Angeles, CA 90095, USA
[b] Department of Electrical Engineering, University of California, Los Angeles, CA 90095, USA

ARTICLE INFO

ABSTRACT

This work focuses on modeling and control of aggregate thin film surface morphology for improved light trapping using a patterned deposition rate profile. The dynamics of the evolution of the thin film surface height profile are modeled by an Edwards–Wilkinson-type equation (a second-order stochastic partial differential equation) in two spatial dimensions. The thin film surface morphology is characterized in terms of aggregate surface roughness and surface slope. These variables are computed with respect to appropriate visible light-relevant characteristic length scales and defined as the root-mean-squares of height deviation and slope of aggregate surface height profiles, respectively. Analytical solutions of the expected aggregate surface roughness and surface slope are obtained by solving the Edwards–Wilkinson equation and are used in the controller design. The model parameters of the Edwards–Wilkinson equation are estimated from kinetic Monte-Carlo simulations using a novel parameter estimation procedure. This parameter dependence on the deposition rate is used in the formulation of the predictive controller to predict the influence of the control action on the surface roughness and slope at the end of the growth process. The cost function of the controller involves penalties on both aggregate surface roughness and mean slope from set-point values as well as constraints on the magnitude and rate of change of the control action. The controller is applied to the two-dimensional Edwards–Wilkinson equation. Simulation results show that the proposed controller successfully regulates aggregate surface roughness and slope to set-point values at the end of the deposition that yield desired levels of thin film reflectance and transmittance.

© 2011 Elsevier Ltd. All rights reserved.

1. Introduction

Photovoltaic (solar) cells are an important source of sustainable energy. Thin film silicon solar cells are currently among the most important and widely used solar cells and their share of the overall solar cell market is steadily increasing (e.g., Green, 2007; van Sark et al., 2007). Research on optical modeling of thin film silicon solar cells indicates that the scattering properties of the thin film interfaces directly influence the light trapping process and the efficiencies of thin film silicon solar cells (e.g., Zeman and Vanswaaij, 2000; Poruba et al., 2000; Müller et al., 2004; Springer and Poruba, 2004; Rowlands et al., 2004). For example, a higher diffused transmittance of incident light is desired for the upper surface of solar cells for a maximum energy input. The scattering properties of the interfaces have a complex correlation with the surface morphology; in particular, the root-mean-square roughness

and slope (Vorburger et al., 1993) at characteristic length scales that are comparable to the wavelength of the visible light. Specifically, significant increase of conversion efficiency with appropriately roughened interfaces has been reported in several works (Tao and Zeman, 1994; Leblanc and Perrin, 1994; Springer et al., 2001; Krč and Zeman, 2002). However, no efforts have been seen in improving the conversion efficiency of thin film solar cells via the regulation of the thin film surface morphology during the manufacturing process by appropriately tailoring the surface slope and roughness to desired specifications. Thus, it is desirable to develop systematic approaches to manufacture thin film solar cells with optimal conversion efficiencies via computational multiscale modeling and real-time model-based control of the manufacturing process.

In the context of modeling of thin film surface morphology and microstructure, mathematical modeling techniques have been developed to describe the microscopic features of thin film growth including: (1) kinetic Monte-Carlo (kMC) methods (e.g., Gillespie, 1976; Reese et al., 2001), and (2) stochastic partial differential equations (Edwards and Wilkinson, 1982; Vvedensky et al., 1993; Lauritsen et al., 1996). In addition to microscopic modeling, real-time feedback control of deposition conditions,

* Corresponding author at: Department of Chemical and Biomolecular Engineering, University of California, Los Angeles, CA 90095, USA. Tel.: +1 310 794 1015; fax: +1 310 206 4107.
E-mail address: pdc@seas.ucla.edu (P.D. Christofides).

based on mathematical models, has become increasingly important in order to meet stringent requirements on thin film quality and reduce thin film variability. While deposition uniformity and composition control can be accomplished on the basis of continuum-type distributed parameter models, precise control of thin film microstructure requires multiscale distributed models that predict how the film state on the microscopic level is affected by changes in the controllable process parameters. Since kMC models are not available in closed form, they cannot be readily used for feedback control design and system-level analysis. On the other hand, stochastic differential equation (SDE) models can be derived from the corresponding master equation of the microscopic process and/or identified from process data (Christofides et al., 2008; Ni and Christofides, 2005). The closed form of the SDE models enables their use as the basis for the design of feedback controllers which can regulate thin film surface roughness (e.g., Christofides et al., 2008; Ni and Christofides, 2005; Hu et al., 2009d), film porosity (Hu et al., 2009b, 2009d), and film thickness (Hu et al., 2009c). Recently, we have initiated an effort towards modeling and control of thin film surface morphology to optimize the light reflectance and transmittance properties of thin films. In this direction, we have studied the dynamics and lattice size dependence of surface mean slope (Huang et al., 2011) and have developed predictive control algorithms to regulate both surface roughness and slope at an atomic level using stochastic PDEs in one spatial dimension (Zhang et al., 2010c) and two spatial dimensions (Zhang et al., 2010b). However, control of thin film surface morphology at a length scale comparable to the visible light wavelength has remained an unsolved practical problem.

This work focuses on modeling and control of aggregate thin film surface morphology for improved light trapping using a patterned deposition rate profile. The dynamics of the evolution of the thin film surface height profile are modeled by an Edwards–Wilkinson-type equation (a second-order stochastic partial differential equation) in two spatial dimensions. It is first established that the use of a spatially uniform deposition rate profile cannot generate significant thin film surface roughness and slope at large length scales (comparable to visible light wavelength), necessitating the use of a sine-wave-patterned deposition rate profile in space. The thin film surface morphology is described in terms of aggregate surface roughness and surface slope, computed with respect to appropriate visible light-relevant characteristic length scales and defined as the root-mean-squares of an aggregate surface height profile and of an aggregate surface slope profile, respectively. Using analytical solutions of the expected aggregate surface roughness and surface slope, the functional dependence of the Edwards–Wilkinson equation model parameters on the deposition rate is computed and used within a predictive control framework to predict the influence of the control action on the surface roughness and slope at the end of the growth process. The controller is applied to the two-dimensional Edwards–Wilkinson equation representing an 8000 nm × 8000 nm spatial domain and using a sine-wave-patterned deposition rate profile in space, and it is shown to successfully regulate aggregate surface roughness and slope at the end of the deposition at levels that yield desired thin film reflectance and transmittance levels.

2. Aggregate surface morphology

2.1. Process description and modeling

In this work, the thin film deposition process is modeled by an on-lattice kinetic Monte-Carlo model. Details of the model can be found in previous work of our group (Huang et al., 2010). The two dimensional square lattice where the deposition process takes
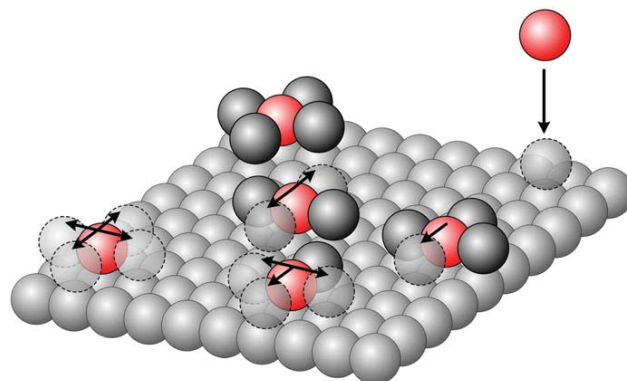

Fig. 1. Thin film deposition process on a 2D square lattice.

place is shown in Fig. 1. Periodic boundary conditions (PBCs) are applied in the directions perpendicular to the growth direction. Two different types of micro-processes are considered: an adsorption process and a migration process. In the adsorption process, incident particles are incorporated onto the thin film. The incidence direction in the adsorption process is restricted to be the vertical direction. The rate of adsorption is proportional to the average deposition rate across the simulation domain. The site in which a particle is deposited is randomly selected from all lattice sites with equal probability. During the migration process, particles on the thin film surface hop against appropriate energy barriers and move to their vacant neighboring sites. The migration rate follows an Arrhenius-type law and depends on the local particle micro-configuration (i.e., number of nearest neighboring particles). The substrate temperature is fixed at 460 K. The lattice is initialized with a fully packed and fixed substrate. A continuous-time Monte-Carlo (CTMC)-type algorithm (e.g., Vlachos et al., 1993) is used to carry out the simulations.

2.2. Aggregate surface roughness and slope

Thin film surface morphology can be characterized by roughness and slope. Roughness is defined as the root-mean-square (RMS) of the surface height profile

$$r(t) = \sqrt{\frac{1}{L^2} \int_0^L \int_0^L (h(x,y,t) - \bar{h}(t))^2 \, dx \, dy}$$

$$\approx \sqrt{\frac{1}{l^2} \sum_{i=0}^{l-1} \sum_{j=0}^{l-1} (h(i,j,t) - \bar{h})^2}, \tag{1}$$

where $h(i,j,t)$ is the surface height measurement at the (i,j) lattice site at time t, $\bar{h}$ denotes the average surface height, L is the dimension of the simulation domain, l is the number of discrete height measurements on x or y direction. Slope is defined as the root-mean-square of the gradient of the surface height in x direction

$$m(t) = \sqrt{\frac{1}{L^2} \int_0^L \int_0^L \left(\frac{\partial h}{\partial x}(x,y,t)\right)^2 dx \, dy}$$

$$\approx \sqrt{\frac{1}{L^2} \sum_{i=0}^{l-1} \sum_{j=0}^{l-1} \left(\frac{h(i+1,j,t) - h(i,j,t)}{\Delta x}\right)^2 \frac{L^2}{l^2}}$$

$$= \sqrt{\frac{1}{l^2} \sum_{i=0}^{l-1} \sum_{j=0}^{l-1} (h(i+1,j,t) - h(i,j,t))^2}. \tag{2}$$
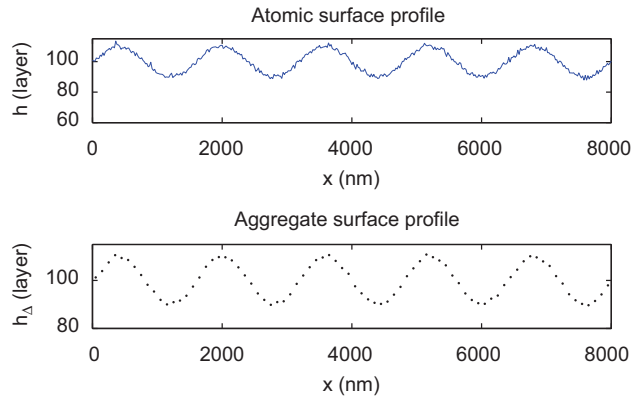
Fig. 2. 1D surface with roughness at different length scales: atomic surface profile (top plot) and aggregate surface profile (bottom plot).

Roughness and slope can be defined at different length scales. The top subplot in Fig. 2 shows a one-dimensional (1D) surface with roughness at different length scales. In order to characterize surface morphology at different length scales, an aggregate surface height profile $h_\Delta(i,j)$ is introduced in this work. The aggregate surface height profile is the averaged height over an interval of length Δ in 1D and a square of side Δ in 2D. In the 2D case, the aggregate surface height takes the form

$$h_\Delta(i,j) = \frac{\sum_{i_a=0}^{\Delta-1} \sum_{j_a=0}^{\Delta-1} h(i\Delta + i_a, j\Delta + j_a)}{\Delta^2}, \quad i,j = 0,1,2,\ldots,l_\Delta - 1, \quad (3)$$

where l_Δ is the number of points on the discrete aggregate surface height profile. Then the aggregate surface roughness, r_Δ, and the aggregate surface slope, m_Δ, can be defined based on the aggregate surface height profile as follows

$$r_\Delta(t) = \sqrt{\frac{1}{l_\Delta^2} \sum_{i=0}^{l_\Delta-1} \sum_{j=0}^{l_\Delta-1} (h_\Delta(i,j,t) - \overline{h}_\Delta(t))^2}, \quad (4)$$

$$m_\Delta(t) = \sqrt{\frac{1}{l^2} \sum_{i=0}^{l_\Delta-1} \sum_{j=0}^{l_\Delta-1} (h_\Delta(i+1,j,t) - h_\Delta(i,j,t))^2}. \quad (5)$$

Remark 1. Fig. 2 shows an example of an atomic surface profile and of an aggregate surface profile. We note that in general the surface morphology, including roughness and slope, depends on lattice size and this dependence has been explored in other works of our group (the reader may refer to Hu et al. (2009a) and Huang et al. (2010, 2011)).

2.3. Light reflection on a rough surface

For thin film solar cells, the energy conversion efficiency is directly related to the light trapping/scattering properties of the thin film interfaces and surfaces, which in turn depend on the surface roughness and slope. It should be pointed out that the wavelength of visible light (380–750 nm) is several orders of magnitude greater than the distance between two neighboring atoms (≈ 0.2 nm). The light reflection depends on roughness and slope defined at a length scale comparable to the light wavelength.

When incident light goes through a rough interface, it is divided into four components: specular reflection, specular transmission, diffused reflection and diffused transmission (Tao and Zeman, 1994; Leblanc and Perrin, 1994). If a rough thin film surface is illuminated with a beam of monochromatic light at normal incidence, the total reflectance, R, can be approximated as follows (Davies, 1954):

$$R = R_0 \exp\left[-\frac{4\pi r_\Delta^2}{\lambda^2}\right] + R_0 \int_0^{\pi/2} 2\pi^4 \left(\frac{a_\Delta}{\lambda}\right)^2 \left(\frac{r_\Delta}{\lambda}\right)^2$$

$$\cdot (\cos\theta + 1)^4 \sin\theta \exp\left[-\frac{(\pi a_\Delta \sin\theta)^2}{\lambda^2}\right] d\theta, \quad (6)$$

where R_0 is the reflection of a perfectly smooth surface, r_Δ is the aggregate surface roughness, θ is the reflectance angle, λ is the light wavelength and a_Δ is the auto-covariance length of the surface. It can be proved that $a_\Delta = \sqrt{2} r_\Delta / m_\Delta$, where m_Δ is the slope of the aggregate profile of the surface (Bennett and Porteus, 1961). The numerical integration result of Eq. (6) is shown in Fig. 3 using $\lambda = 700$ nm. Both r_Δ and m_Δ strongly influence the intensity of light reflection (and therefore, light transmission) of the surface/interface. Thus, it is important to regulate r_Δ and m_Δ of the surfaces/interfaces of the thin film solar cells to appropriate values that optimize light reflection and transmission during thin film manufacturing.

2.4. Patterned deposition rate profile

Fig. 4 shows the variation of roughness and slope as a function of aggregation length for a deposition process with uniform deposition rate profile. The results are from a kinetic Monte-Carlo simulation of the two-dimensional thin film deposition process of Fig. 1 with $l = 200$. Both aggregate roughness and slope decrease as aggregation length increases. In this case, the surface roughness is due to atomic level fluctuations and thus we conclude that atomic level fluctuations contribute mainly to roughness and slope at small length scales.

In order to generate significant roughness and slope at large length scales (i.e., comparable to the wave length of visible light), we introduce a patterned deposition rate profile of the following form:

$$w(x,y,t) = w_0(t) + A(t) \sin\left(\frac{2k\pi}{L}x\right), \quad (7)$$

where w_0 is the mean deposition rate across the simulation domain, A is the magnitude of the sine wave, k is the number of complete
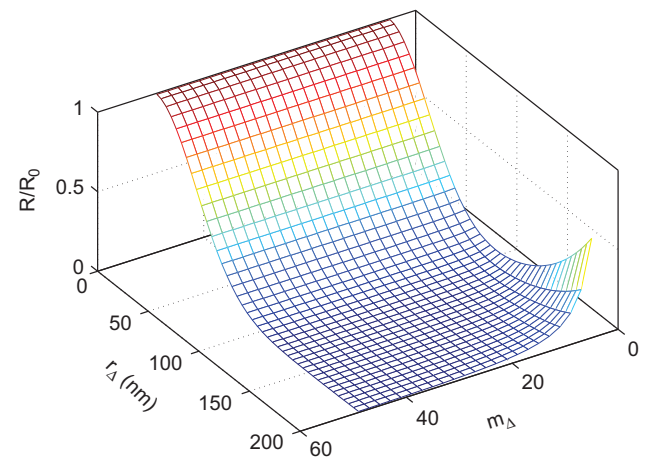

Fig. 3. Reflection as a function of r_Δ and m_Δ of thin film surface.
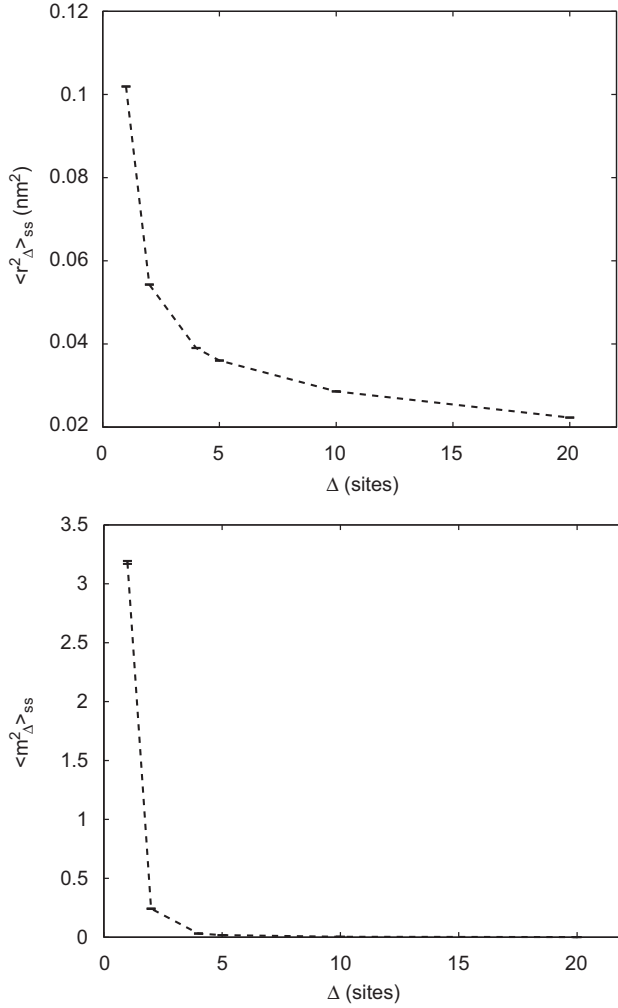
Fig. 4. Dependence of the steady state values of aggregate roughness (top plot) and aggregate slope (bottom plot) on aggregation length.

periods of the sine wave within the simulation domain, and L is the length of the simulation domain.

2.5. Edwards–Wilkinson equation for surface height dynamics

To design a feedback controller for the thin film deposition process, a closed form model is needed. The Edwards–Wilkinson (EW) equation, which is a second-order stochastic partial differential equation (PDE), has been demonstrated to adequately describe the dynamics of the evolution of the surface height profile in many thin film growth processes that involve a thermal balance between atom adsorption and surface migration (Edwards and Wilkinson, 1982; Family, 1986; Hu et al., 2009a; Huang et al., 2011). In this work, we consider a two dimensional (2D) EW type equation of the following form:

$$\frac{\partial h_\Delta}{\partial t} = w(x,y,t) + c_2\left(\frac{\partial^2 h_\Delta}{\partial x^2} + \frac{\partial^2 h_\Delta}{\partial y^2}\right) + \xi(x,y,t), \tag{8}$$

where $x \in [0,L]$, $y \in [0,L]$ are the spatial coordinates, t is the time, $h_\Delta(x,y,t)$ is the aggregate surface height, and $\xi(x,y,t)$ is a Gaussian white noise with zero mean and covariance:

$$\langle \xi(x,y,t)\xi(x',y',t') \rangle = \sigma^2 \delta(x-x')\delta(y-y')\delta(t-t'). \tag{9}$$

where $\delta(\cdot)$ denotes the Dirac delta function, $w(x,y,t)$ is the patterned deposition rate profile described in Eq. (7), and c_2 and σ^2 are model parameters that depend on the mean deposition rate, w_0. The stochastic PDE of Eq. (8) is subject to the following periodic boundary conditions:

$$h_\Delta(0,y,t) = h_\Delta(L,y,t), \quad h_\Delta(x,0,t) = h_\Delta(x,L,t), \tag{10}$$

$$\frac{\partial h_\Delta}{\partial x}(0,y,t) = \frac{\partial h_\Delta}{\partial x}(L,y,t), \quad \frac{\partial h_\Delta}{\partial y}(x,0,t) = \frac{\partial h_\Delta}{\partial y}(x,L,t), \tag{11}$$

and the initial condition

$$h_\Delta(x,y,0) = h_{0\Delta}(x,y) \tag{12}$$

To analyze the dynamics and obtain a finite-dimensional approximation of the EW equation, we first consider the eigenvalue problem of the linear operator of Eq. (8) subject to the periodic boundary conditions of Eqs. (10) and (11):

$$\mathcal{A}\phi_{n_x,n_y}(x,y) = c_2\left(\frac{\partial^2}{\partial x^2} + \frac{\partial^2}{\partial y^2}\right)\phi_{n_x,n_y}(x,y) = \lambda_{n_x,n_y}\phi_{n_x,n_y}(x,y), \tag{13}$$

$$\nabla^j\phi_{n_x,n_y}(0,y) = \nabla^j\phi_{n_x,n_y}(L,y), \quad j = 0,1 \tag{14}$$

$$\nabla^j\phi_{n_x,n_y}(x,0) = \nabla^j\phi_{n_x,n_y}(x,L), \quad j = 0,1 \tag{15}$$

where λ_{n_x,n_y} denotes an eigenvalue, ϕ_{n_x,n_y} denotes an eigenfunction, and ∇^j, $j=0$, 1, denotes the value and gradient of a given function, respectively. The solution of the eigenvalue problem is as follows:

$$\lambda_{n_x,n_y} = -\frac{4c_2\pi^2}{L^2}(n_x^2 + n_y^2), \tag{16}$$

$$\phi_{1,n_x,n_y} = \frac{2}{L}\sin\left(\frac{2n_x\pi}{L}x\right)\sin\left(\frac{2n_y\pi}{L}y\right), \tag{17}$$

$$\phi_{2,n_x,n_y} = \begin{cases} \frac{1}{L}, & n_x = 0 \text{ and } n_y = 0, \\ \frac{2}{L}\cos\left(\frac{2n_x\pi}{L}x\right)\cos\left(\frac{2n_y\pi}{L}y\right), & n_x \neq 0 \text{ and } n_y \neq 0, \\ \frac{\sqrt{2}}{L}\cos\left(\frac{2n_x\pi}{L}x\right)\cos\left(\frac{2n_y\pi}{L}y\right) & \text{otherwise,} \end{cases} \tag{18}$$

$$\phi_{3,n_x,n_y} = \begin{cases} 0 & n_x = 0, \\ \frac{2}{L}\sin\left(\frac{2n_x\pi}{L}x\right)\cos\left(\frac{2n_y\pi}{L}y\right) & n_x \neq 0, \ n_y \neq 0, \\ \frac{\sqrt{2}}{L}\sin\left(\frac{2n_x\pi}{L}x\right) & n_x \neq 0, \ n_y = 0, \end{cases} \tag{19}$$

$$\phi_{4,n_x,n_y} = \begin{cases} 0 & n_y = 0, \\ \frac{2}{L}\cos\left(\frac{2n_x\pi}{L}x\right)\sin\left(\frac{2n_y\pi}{L}y\right) & n_y \neq 0, \ n_x \neq 0, \\ \frac{\sqrt{2}}{L}\sin\left(\frac{2n_y\pi}{L}y\right) & n_y \neq 0, \ n_x = 0. \end{cases} \tag{20}$$

The solution of the EW equation of Eq. (8) can be expanded in an infinite series in terms of the eigenfunctions of the operator of Eq. (13) as follows:

$$h_\Delta(x,y,t) = \sum_{n_x=0}^{+\infty} \sum_{n_y=0}^{+\infty} \sum_{p=1}^{4} \phi_{p,n_x,n_y}(x,y)z_{p,n_x,n_y}(t), \tag{21}$$

where $z_{p,n_x,n_y}(t)$, $p = 1,2,3,4$, are time-varying coefficients.

Substituting the above expansion of $h_\Delta(x,y,t)$ into Eq. (8) and taking the inner product with the adjoint eigenfunctions, the following system of infinite stochastic linear ordinary differential equations (ODEs) for the temporal evolution of the time-varying

coefficients is obtained:

$$\frac{dz_{2,0,0}}{dt} = w_{2,0,0} + \xi_{2,0,0}(t), \tag{22}$$

$$\frac{dz_{p,n_x,n_y}}{dt} = w_{p,n_x,n_y} + \lambda_{n_x,n_y} z_{p,n_x,n_y} + \xi_{p,n_x,n_y}(t), \tag{23}$$

$$p = 1,2,3,4, \quad n_x, n_y = 0,1,\ldots,\infty, \quad n_x^2 + n_y^2 \neq 0,$$

where $\xi_{p,n_x,n_y}(t) = \int_0^L \int_0^L \xi(x,y,t)\phi_{p,n_x,n_y}(x,y)\,dx\,dy$ is the projection of the noise $\xi(x,y,t)$ on the ODE for z_{p,n_x,n_y}. The noise term, ξ_{p,n_x,n_y}, has zero mean and covariance

$$\langle \xi_{p,n_x,n_y}(t)\xi_{p,n_x,n_y}(t') \rangle = \sigma^2 \delta(t-t'). \tag{24}$$

Similarly, w_{p,n_x,n_y} is the projection of w on the ODE for z_{p,n_x,n_y}:

$$w_{p,n_x,n_y} = \int_0^L \int_0^L \phi_{p,n_x,n_y}(x,y)w(x,y)\,dx\,dy, \tag{25}$$

$$w_{1,n_x,n_y} = 0, \tag{26}$$

$$w_{2,n_x,n_y} = \begin{cases} w_0 L + \dfrac{AL}{2k\pi}[1-\cos(2k\pi)] & n_x = 0, n_y = 0, \\ \dfrac{\sqrt{2}ALk}{2\pi(n_x^2-k^2)}[\cos(2k\pi)-1] & n_x \neq 0, n_x \neq k, n_y = 0, \\ 0 & \text{otherwise.} \end{cases} \tag{27}$$

$$w_{3,n_x,n_y} = \begin{cases} \dfrac{\sqrt{2}AL}{2} & n_x = k, n_y \neq 0, \\ \dfrac{\sqrt{2}ALn_x}{2\pi(k^2-n_x^2)}\sin(2k\pi) & n_x \neq 0, n_x \neq k, n_y = 0, \\ 0 & \text{otherwise,} \end{cases} \tag{28}$$

$$w_{4,n_x,n_y} = 0. \tag{29}$$

The temporal evolution of the variance of mode z_{p,n_x,n_y} can be obtained from the solution of the linear ODEs of Eqs. (22) and (23) as follows:

$$\langle z_{2,0,0}(t) \rangle = w_{2,0,0}(t-t_0), \tag{30}$$

$$\mathrm{var}(z_{2,0,0}(t)) = \sigma^2(t-t_0), \tag{31}$$

$$\langle z(t) \rangle = e^{\lambda(t-t_0)}\langle z(t_0) \rangle + \frac{w_p}{\lambda}(e^{\lambda(t-t_0)}-1), \tag{32}$$

$$\mathrm{var}(z(t)) = e^{2\lambda(t-t_0)}\mathrm{var}(z(t_0)) + \sigma^2 \frac{e^{2\lambda(t-t_0)}-1}{2\lambda}, \tag{33}$$

where $z(t) = z_{p,n_x,n_y}(t)$ and $w_p = w_{p,n_x,n_y}$ for $n_x^2 + n_y^2 \neq 0$.

For feedback control purposes (see Section 3 below), the modes can be calculated from a surface height measurement as follows:

$$z_{p,n_x,n_y}(t) = \int_0^L \int_0^L h_\Delta(x,y,t)\phi_{p,n_x,n_y}(x,y)\,dx\,dy. \tag{34}$$

In many circumstances, only discrete height profile point measurements are available, thus Eq. (34) can be approximated by

$$z_{p,n_x,n_y}(t) \approx \left(\frac{L}{l_\Delta}\right)^2 \sum_{i=0}^{l_\Delta-1}\sum_{j=0}^{l_\Delta-1} h_\Delta(i,j,t)\phi_{p,n_x,n_y}(i,j), \tag{35}$$

where l_Δ is the number of spatial height sampling (measurement) points in [0,L]. It is worth pointing out that, when discrete height point measurements are available, the largest number of modes that can be accurately calculated is limited by the spatial sampling points, i.e. $n_x, n_y \leq l_\Delta/2$ (Zhang et al., 2010b).

Substituting Eq. (21) into Eq. (4), the expected value of r_Δ^2 can be rewritten in terms of the state covariance as follows:

$$\langle r_\Delta^2 \rangle = \frac{1}{L^2} \sum_{\substack{n_x,n_y=0 \\ n_x^2+n_y^2 \neq 0}}^{\infty} \sum_{p=1}^{4} \langle z_{p,n_x,n_y}^2 \rangle. \tag{36}$$

The expected RMS slope square can also be expressed in terms of the state covariance as follows:

$$\langle m_\Delta^2 \rangle = \sum_{\substack{n_x,n_y=0 \\ n_x^2+n_y^2 \neq 0}}^{\infty} \sum_{p=1}^{4} K_{p,n_x,n_y} \langle z_{p,n_x,n_y}^2 \rangle, \tag{37}$$

where K_{p,n_x,n_y} can be computed by

$$K_{p,n_x,n_y} = \frac{1}{L^2}\sum_{i=0}^{l_\Delta-1}\sum_{j=0}^{l_\Delta-1}(\phi_{p,n_x,n_y}(i+1,j)-\phi_{p,n_x,n_y}(i,j))^2 = \frac{4l_\Delta^2}{L^4}\sin^2\left(\frac{\pi n_x}{l_\Delta}\right). \tag{38}$$

2.6. Determination of model parameters

The EW equation has two parameters, c_2 and σ^2, which are assumed to depend on the mean deposition rate w_0. In our previous work (Zhang et al., 2010a), the dependencies of EW equation parameters on operating conditions were found by fitting the analytical solution of $\langle r^2 \rangle$ to open-loop kinetic Monte-Carlo simulations. However, this approach is not applicable here because a system with a much larger physical domain is simulated. Assuming the distance between two neighboring sites is 0.2 nm, there are 40 000 × 40 000 sites within the 8000 nm × 8000 nm square domain that is simulated. Since it is not possible to simulate such large lattice size directly, we use the following steps to get estimates of c_2 and σ^2 as functions of w_0.

1. For each value of w_0, a series of open-loop kinetic Monte-Carlo simulations is carried out with increasing lattice size (l=20, 50,100,150,200,250). The values of c_2 and σ^2 are then determined by fitting the analytical solution of $\langle r^2(t) \rangle$ (without any aggregation) to kMC simulation data using the least square method. As a result, c_2 and σ^2 as functions of lattice size l are obtained for each value of w_0, as shown in Fig. 5. The following functional forms are used for the fitting of c_2 and σ^2/c_2:

   $$c_2(l,w_0) = a_c(w_0)l + b_c(w_0), \tag{39}$$

   $$\frac{\sigma^2}{c_2}(l,w_0) = a_s(w_0)\log_{10}(l) + b_s(w_0), \tag{40}$$

   where the values of the coefficients $a_c(w_0)$, $b_c(w_0)$, $a_s(w_0)$ and $b_s(w_0)$ for different w_0 values are given in Table 1.
2. The values of c_2 and σ^2 at lattice size l=40 000 are determined by extrapolating the c_2 and σ^2 according to Eqs. (39) and (40). The extrapolated values $c_2(l$=40 000$,w_0)$ and $\sigma^2(l$=40 000$,w_0)$ are also included in Table 1.
3. Subsequently, we fit the extrapolated values of c_2 and σ^2 for l=40 000 as functions of w_0, as shown in Fig. 6. The following functional forms for $c_2(w_0)$ and $\sigma^2(w_0)$ are used:

   $$c_2(w_0) = p_{c1}w_0^3 + p_{c2}w_0^2 + p_{c3}w_0 + p_{c4}, \tag{41}$$

   $$\sigma^2(w_0) = p_{s1}w_0^4 + p_{s2}w_0^3 + p_{s3}w_0^2 + p_{s4}w_0 + p_{s5}, \tag{42}$$

   where

   $$p_{c1} = -20.83, \quad p_{c2} = 110.9, \quad p_{c3} = -204.1, \quad p_{c4} = 164.9, \tag{43}$$

   $$p_{s1} = -7.585, \quad p_{s2} = 36.65, \quad p_{s3} = -59.03,$$

   $$p_{s4} = 42.91, \quad p_{s5} = 2.998. \tag{44}$$

To verify the above approach, we compare the roughness obtained from the extrapolated values of c_2 and σ^2 with that from

direct extrapolation of $\langle r^2 \rangle$. First, $\langle r^2 \rangle$ is extrapolated with respect to lattice size and its value at $l = 40\,000$ is obtained. Fig. 7 shows the steady state value of $\langle r^2 \rangle$ against lattice size. According to Fig. 7, $\langle r^2 \rangle$ can be fitted to a linear function of $\log_{10}(l)$ of the form:

$$\langle r^2 \rangle_{ss}(l) = a_r \log_{10}(l) + b_r. \tag{45}$$

Then the relationship between steady state roughness and aggregation length, as shown in Fig. 8, is used to find the roughness with aggregation length $\Delta = 400$. $\langle r_\Delta^2 \rangle(\Delta)$ is fitted to a power-law function of the form:

$$\langle r_\Delta^2 \rangle(\Delta) = a_a \Delta^{b_a} + c_a, \tag{46}$$

where $a_a = 0.07883$, $b_a = -1.193$ and $c_a = 0.02247$. According to Eq. (46), $\langle r_\Delta^2 \rangle(\Delta = 400) = 0.2224 \langle r_\Delta^2 \rangle(\Delta = 1)$, thus the aggregate

roughness for lattice size $l = 40\,000$ and aggregation length $\Delta = 400$ can be calculated. The results are summarized in Table 2.

Subsequently, we use the extrapolated values of σ^2/c_2 to calculate the atomic and aggregate steady state surface roughness. According to Eq. (36), the steady state roughness of a deposition process starting from a flat surface would be

$$\langle r_\Delta^2 \rangle_{ss} = \frac{1}{L^2} \sum_{\substack{n_x, n_y = 0 \\ n_x^2 + n_y^2 \neq 0}}^{\infty} \sum_{p=1}^{4} \langle z_{p,n_x,n_y}^2 \rangle = \frac{1}{L^2} \sum_{\substack{n_x, n_y = 0 \\ n_x^2 + n_y^2 \neq 0}}^{\infty} \sum_{p=1}^{4} \mathrm{var}(z_{p,n_x,n_y})$$

$$= \frac{\sigma^2}{c_2 L^2} \sum_{\substack{n_x, n_y = 0 \\ n_x^2 + n_y^2 \neq 0}}^{\infty} \frac{L^2}{2\pi^2(n_x^2 + n_y^2)} = \frac{\sigma^2}{c_2} \sum_{\substack{n_x, n_y = 0 \\ n_x^2 + n_y^2 \neq 0}}^{\infty} \frac{1}{2\pi^2(n_x^2 + n_y^2)} \approx 0.4353 \frac{\sigma^2}{c_2}. \tag{47}$$
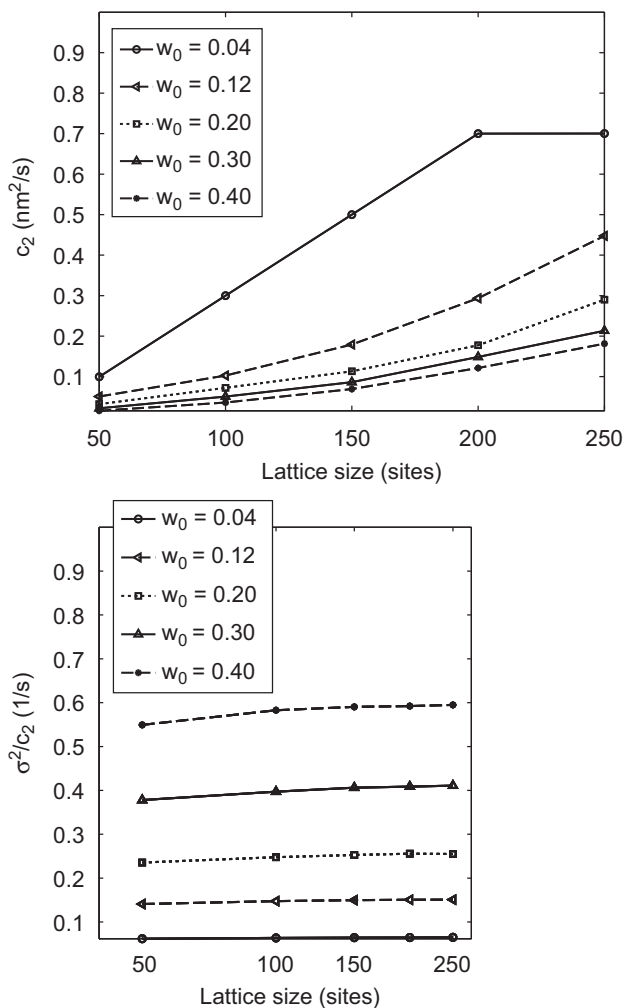
The results are shown in Table 3.

Fig. 5. c_2 (top plot) and σ_2 (bottom plot) as functions of lattice size l.
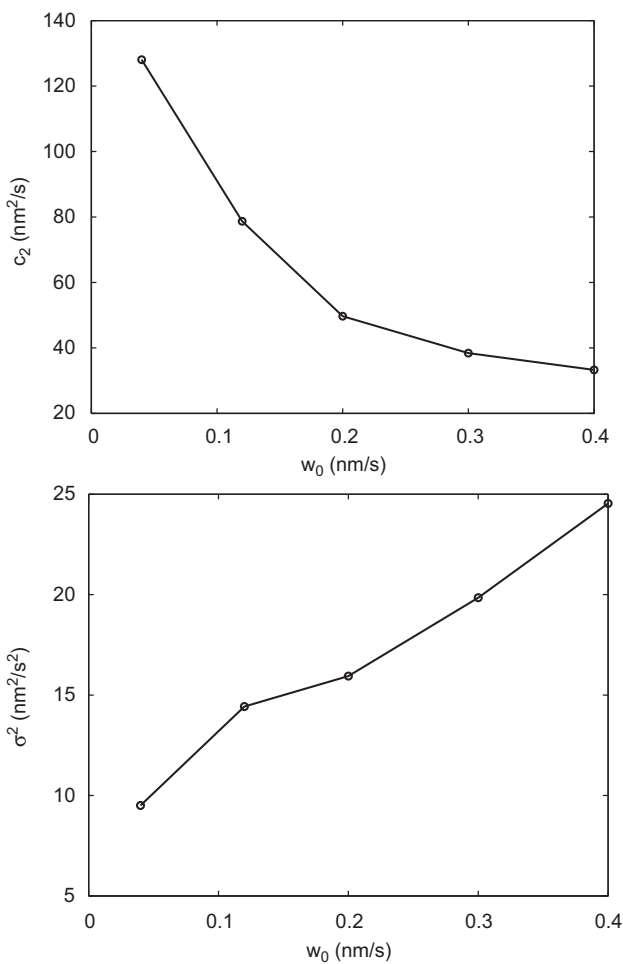

Fig. 6. c_2 (top plot) and σ_2 (bottom plot) as functions of deposition rate w_0.

Table 1
Values of the coefficients used in Eqs. (39) and (40) and the extrapolated values of c_2 and σ^2 for lattice size $l = 40\,000$.

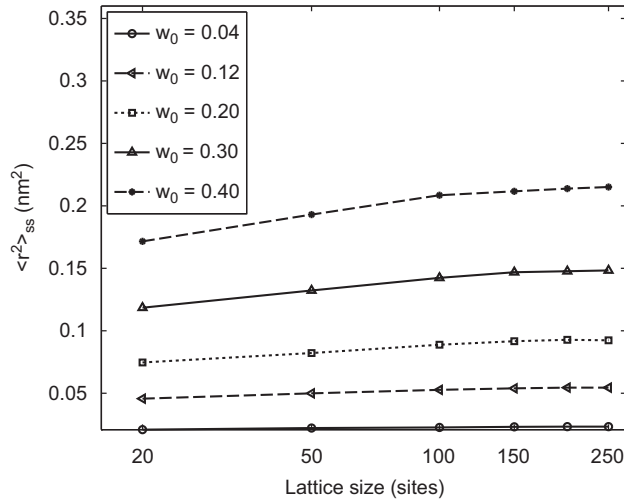| w_0	a_c	b_c	c_2	a_s	b_s	σ^2
0.04	3.20×10^{-3}	-3.04×10^{-2}	128.06	4.17×10^{-3}	5.50×10^{-2}	9.50
0.12	1.97×10^{-3}	-7.16×10^{-2}	78.67	1.43×10^{-2}	1.17×10^{-1}	14.43
0.20	1.24×10^{-3}	-4.34×10^{-2}	49.67	2.90×10^{-2}	1.87×10^{-1}	15.95
0.30	9.61×10^{-4}	-3.56×10^{-2}	38.42	4.71×10^{-2}	3.00×10^{-1}	19.84
0.40	8.33×10^{-4}	-3.63×10^{-2}	33.28	6.29×10^{-2}	4.48×10^{-1}	24.54

Fig. 7. Steady state value of roughness $\langle r^2 \rangle$ as a function of lattice size l.
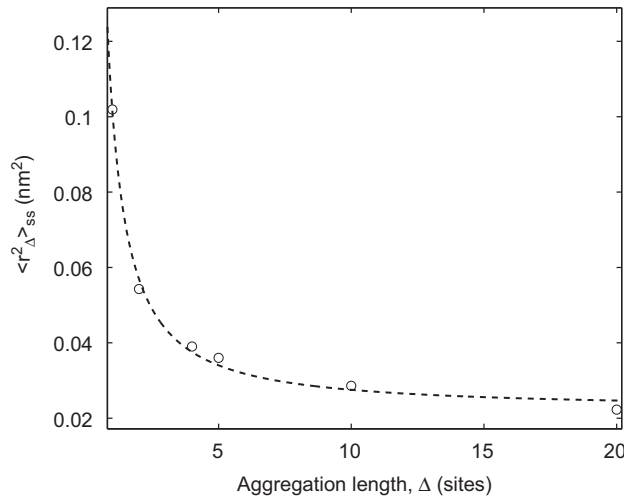

Fig. 8. $\langle r_\Delta^2 \rangle$ as a function of aggregation length Δ (lattice size $l=500$).

Table 2
Extrapolated aggregate roughness when lattice size $l=40\,000$, aggregation length $\Delta = 400$, under different deposition rates.

w_0	a_r	b_r	Roughness $\langle r^2 \rangle_{ss}$ (nm^2)	Aggregate roughness $\langle r_\Delta^2 \rangle_{ss}$ (nm^2)
0.04	0.002143	0.018237	0.0281	6.25×10^{-3}
0.12	0.008171	0.035585	0.0732	1.63×10^{-2}
0.20	0.016950	0.053243	0.1313	2.92×10^{-2}
0.30	0.027590	0.084274	0.2112	4.70×10^{-2}
0.40	0.039788	0.123212	0.3063	6.81×10^{-2}

Comparing Tables 2 and 3, we can see that both approaches yield very close values for both atomic and aggregate surface roughness for $l=40\,000$.

Remark 2. This is the first time the above parameter identification method is proposed. This method could be used for parameter identification for other nonlinear SPDE models, e.g.

Table 3
Calculation of atomic and aggregate steady state surface roughness at lattice size $l=40\,000$ using extrapolated values of σ^2/c_2.

w_0	σ^2/c_2	$\langle r^2 \rangle_{ss}$ (nm^2)	$\langle r_\Delta^2 \rangle_{ss}$ (nm^2)
0.04	0.074187	0.0323	7.18×10^{-3}
0.12	0.183404	0.0800	1.78×10^{-2}
0.20	0.321012	0.1399	3.11×10^{-2}
0.30	0.516476	0.2551	5.67×10^{-2}
0.40	0.737238	0.3214	7.15×10^{-2}

Kuramoto–Sivashinsky equation (KSE), which describe surface evolution in other thin film growth models.

3. Predictive controller design

In this section, a model predictive controller is developed based on the dynamic model of the expected roughness square and slope square. The mean deposition rate, w_0, and magnitude of sine wave, A, are used as the manipulated variables. In this work, state feedback is used. At each sampling time, the surface height profile from the stochastic PDE is fed-back to the controller and the eigenmodes are calculated. In practice, real-time surface height measurements can be obtained via atomic force microscopy (AFM) systems. The control objective is to minimize the deviation of the expected roughness square and slope square from desired set-point values. Because the thin film deposition process is a batch process, the interval between current time and the end of the batch run is used as the prediction horizon. During each predictive controller evaluation, the manipulated variable is assumed to stay fixed until the end of the batch. The constraints of the problem are (1) the mean deposition rate has lower and upper limits; (2) the rate of change of the mean deposition rate should be less than an upper limit due to actuator limitations; (3) the magnitude of sine wave should be positive and smaller than the average deposition rate. The resulting MPC formulation is as follows:

$$\min_{w_0, A} f(w_0, A) = q_{r^2} \left(\frac{r_{set}^2 - \langle r_\Delta^2(t_f) \rangle}{r_{set}^2} \right)^2 + q_{m^2} \left(\frac{m_{set}^2 - \langle m_\Delta^2(t_f) \rangle}{m_{set}^2} \right)^2, \quad (48)$$

where

$$\langle r_\Delta^2(t_f) \rangle = \frac{1}{L^2} \sum_{\substack{n_x, n_y = 0 \\ n_x^2 + n_y^2 \neq 0}}^{\infty} \sum_{p=1}^{4} \langle z_{p,n_x,n_y}^2(t_f) \rangle, \quad (49)$$

$$\langle m_\Delta^2(t_f) \rangle = \sum_{\substack{n_x, n_y = 0 \\ n_x^2 + n_y^2 \neq 0}} \sum_{p=1}^{4} (K_{p,n_x,n_y} \langle z_{p,n_x,n_y}^2(t_f) \rangle), \quad (50)$$

$$\langle z_{p,n_x,n_y}^2(t_f) \rangle = \mathrm{var}(z_{p,n_x,n_y}(t_f)) + \langle z_{p,n_x,n_y}(t_f) \rangle^2, \quad (51)$$

$$\langle z_{p,n_x,n_y}(t_f) \rangle = e^{\lambda_{n_x,n_y}(t_f - t)} \langle z_{p,n_x,n_y}(t) \rangle + \frac{w_p}{\lambda_{n_x,n_y}} (e^{\lambda_{n_x,n_y}(t_f - t)} - 1), \quad (52)$$

$$\mathrm{var}(z_{p,n_x,n_y}(t_f)) = e^{2\lambda_{n_x,n_y}(t_f - t)} \mathrm{var}(z_{p,n_x,n_y}(t)) + \sigma^2 \frac{e^{2\lambda_{n_x,n_y}(t_f - t)} - 1}{2\lambda_{n_x,n_y}}, \quad (53)$$

$$\lambda_{n_x,n_y} = -\frac{4c_2\pi^2}{L^2}(n_x^2 + n_y^2), \quad n_x^2 + n_y^2 \neq 0. \quad (54)$$

Subject to

$$w_{\min} \leq w_0 \leq w_{\max}, \quad |w_0(t) - w_0(t - dt)| \leq \Delta w_{\max}, \quad (55)$$

$$0 \leq A \leq w_0 \quad (56)$$

where t_f is the final time of the batch run, r_{set}^2 and m_{set}^2 are the respective set-points for the surface roughness square and the

mean slope square, q_{r^2} and q_{m^2} are the weighting factors for the deviations of $\langle r_{\Delta}^2(t_f)\rangle$ and $\langle m_{\Delta}^2(t_f)\rangle$ from their respective set-points, r_{set}^2 and m_{set}^2, dt is the time interval between two successive sampling times, $w_{\min}$ and $w_{\max}$ are the lower and upper bounds on the mean deposition rate, respectively, and $\Delta w_{\max}$ is the limit on the rate of change of the mean deposition rate.

The optimization problem is solved at each sampling time once a new measurement of the surface height profile becomes available. An interior point method optimizer, IPOPT (Wächter and Biegler, 2006), is used to solve the optimization problem in the MPC formulation.

4. Simulation results

In this section, the model predictive controller of Eq. (48) is applied to the two-dimensional EW equation model of Eq. (8). The variation of deposition rate is from 0.02 to 0.4 nm/s, the substrate temperature is fixed at 460 K and the initial deposition rate is 0.2 nm/s; the maximum rate of change of the deposition $\Delta W_{\max} = 0.1$ nm/s. The sampling time is 1 s. Each closed-loop simulation lasts for 100 s. Expected values are calculated from 100 independent closed-loop system simulation runs.

4.1. Control of film surface roughness

First, the problem of regulating film surface roughness is considered. In this scenario, the cost function only contains penalty on the deviation of the expected surface roughness square from the set-point. The weighting factors are $q_{r^2} = 1$ and $q_{m^2} = 0$. The set-point is $r_{set}^2 = 0.04$ nm^2. Because the roughness set-point is small, the surface does not have a clear pattern.

Fig. 9 shows the profile of $\langle r_{\Delta}^2\rangle$ under the model predictive controller of Eq. (48). It can be seen that the controller drives the expected film roughness to the desired value at the end of the simulation. Fig. 10 shows a surface snapshot at the end of the simulation ($t=100$ s) from one single run.

4.2. Control of film surface slope

Next, we consider the regulation of thin film surface slope. The cost function includes only penalty on the deviation of the expected value of slope square from the set point by choosing weighting factors $q_{r^2} = 0$ and $q_{m^2} = 1$. The set point is $m_{set}^2 = 0.025$.
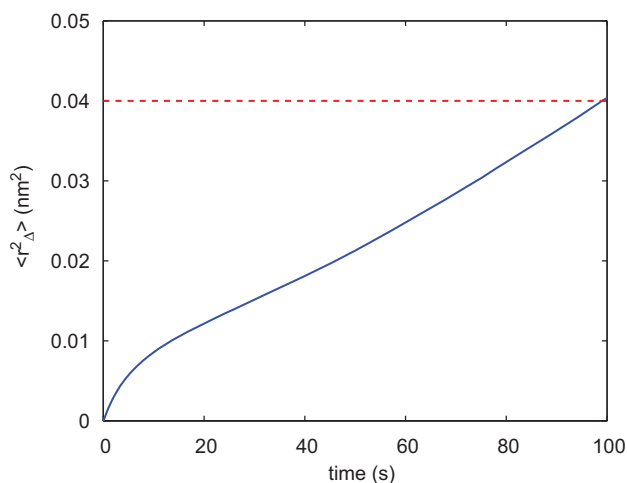
Fig. 9. Profile of expected film surface roughness square from 100 closed-loop simulations. $q_{r^2} = 1$, $q_{m^2} = 0$ and $r_{set}^2 = 0.04$ nm^2.
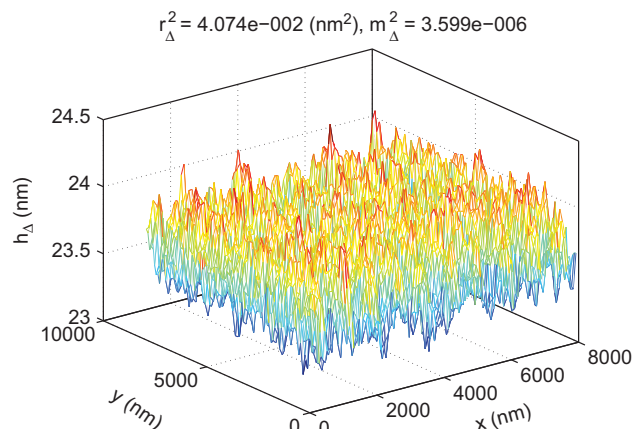
Fig. 10. Surface profile at the end of simulation, $t=100$ s. $q_{r^2} = 1$, $q_{m^2} = 0$ and $r_{set}^2 = 0.04$ nm^2.
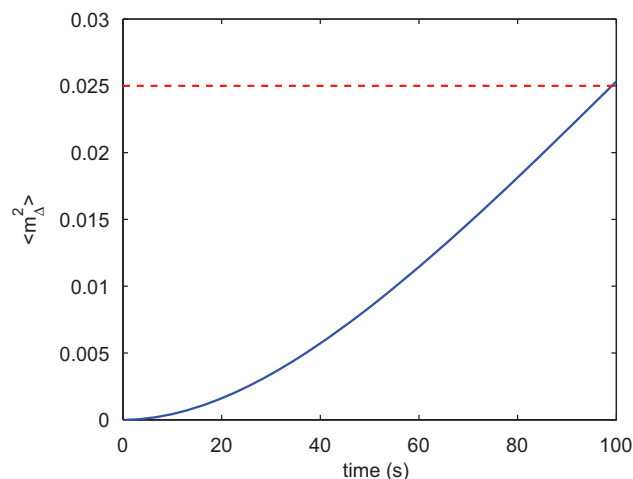
Fig. 11. Profile of expected film surface slope square from 100 closed-loop simulations. $q_{r^2} = 0$, $q_{m^2} = 1$ and $m_{set}^2 = 0.025$.

Fig. 11 shows the profile of the expected slope square. The slope reaches its set point at $t=100$ s. A surface snapshot at $t=100$ s is also given in Fig. 12. The surface in Fig. 12 has clear sine wave pattern because the slope set-point is relatively large for this case.

4.3. Simultaneous control of roughness and slope

Finally, simultaneous regulation of roughness and slope is carried out. The set-points of the surface roughness square and of the mean slope square are $r_{set}^2 = 1.0$ nm^2 and $m_{set}^2 = 0.025$. The weighting factor of mean slope square is kept at 1, while the weighting factor of roughness square increases from 10^{-8} to 1.

Fig. 13 shows the variation of $\langle r_{\Delta}^2\rangle (t=100$ s) and $\langle m_{\Delta}^2\rangle$ $(t=100$ s) as a function of q_{r^2}/q_{m^2}. It can be seen that as the weighting on roughness square increases, the expected roughness square approaches more closely to its set-point value at the cost of larger deviation of slope square from its set-point value and vice versa.
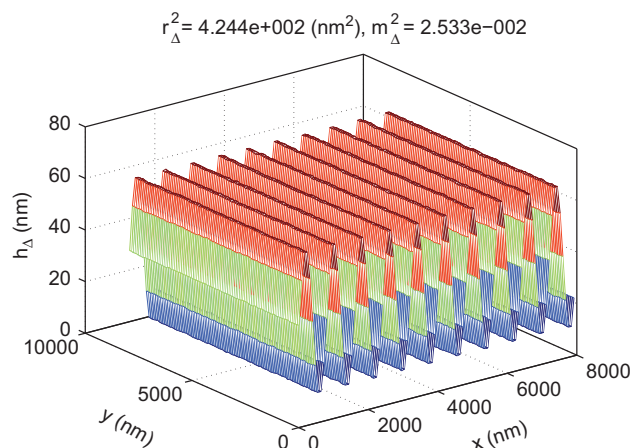
r^2_Δ= 4.244e+002 (nm^2), m^2_Δ = 2.533e−002

Fig. 12. Surface profile at the end of simulation, $t=100$ s. $q_{r^2} = 0$, $q_{m^2} = 1$ and $m^2_{set} = 0.025$.
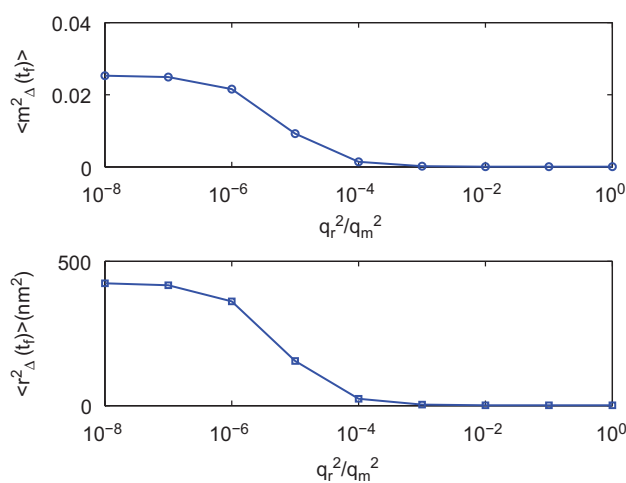

Fig. 13. $\langle r^2_\Delta \rangle$ and $\langle m^2_\Delta \rangle$ at the end of closed-loop simulations ($t=100$ s) for different penalty weighting factors: $q_{m^2} = 1$, $10^{-8} \le q_{r^2} \le 1$, $r^2_{set} = 1.0$, $m^2_{set} = 0.025$.

4.4. Application to light trapping efficiency

We now demonstrate how films of different reflectance can be produced by simultaneous control of film surface roughness and slope. Specifically, the expected surface roughness square and mean slope square can be regulated to different levels by using the same set points and choosing different weighting schemes, i.e., different ratios of the weighting factors, q_{r^2}/q_{m^2}. In particular, q_{m^2} is kept at 1.0 while q_r^2 changes from 10^{-8} to 1. The corresponding light reflectance for different weighting factor ratios can be computed according to Eq. (6). In Fig. 14, the roughness and slope obtained from closed-loop simulations with different q_{r^2}/q_{m^2} are mapped to a contour of reflectance. The points from upper right to lower left correspond to q_{r^2}/q_{m^2} ratios of increasing values. By changing the ratio, q_{r^2}/q_{m^2}, different films can be produced whose surface morphology is characterized by a wide range of reflectance values.

5. Conclusions

In this work, a patterned deposition rate profile was introduced to generate significant roughness and slope at a length
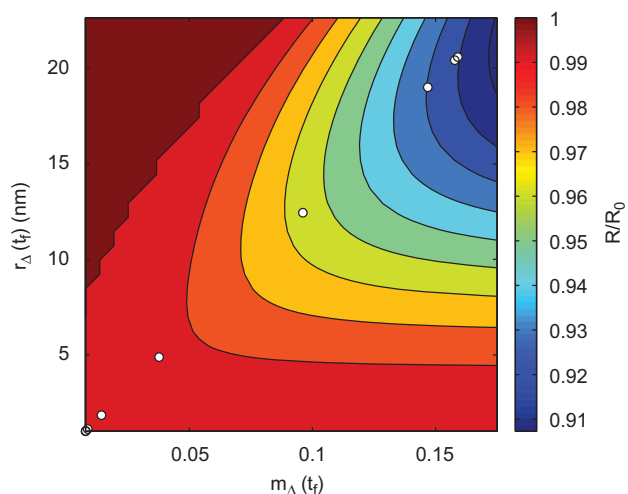

Fig. 14. Light reflectance of thin films deposited under closed-loop operations with different weighting factor ratios: $q_{m^2} = 1$, $10^{-8} \le q_{r^2} \le 1$ (corresponding to points from right to left), $r^2_{set} = 1.0$, $m^2_{set} = 0.025$.

scale comparable to the wavelength of visible light in a thin film deposition process. Working within the framework of the two-dimensional Edwards–Wilkinson equation representing an 8000 nm × 8000 nm spatial domain, a model predictive controller was developed to regulate thin film surface roughness and slope to desired levels, accounting for constraints on the magnitude and rate of change of the control actions. The mean value and magnitude of the sine wave deposition rate profile were used as manipulated variables. Simulation studies demonstrated the applicability and effectiveness of the patterned deposition rate profile and of the controller in successfully regulating the final thin film surface roughness and slope to levels that yield desired thin film reflectance and transmittance.

References

Bennett, H.E., Porteus, J.O., 1961. Relation between surface roughness and specular reflectance at normal incidence. Journal of the Optical Society of America 51, 123–129.

Christofides, P.D., Armaou, A., Lou, Y., Varshney, A., 2008. Control and Optimization of Multiscale Process Systems. Birkhäuser, Boston.

Davies, H., 1954. The reflection of electromagnetic waves from a rough surface. In: Proceedings of the Institution of Electrical Engineers, London 101, 209–214.

Edwards, S.F., Wilkinson, D.R., 1982. The surface statistics of a granular aggregate. Proceedings of the Royal Society of London Series A – Mathematical Physical and Engineering Sciences 381, 17–31.

Family, F., 1986. Scaling of rough surfaces: effects of surface diffusion. Journal of Physics A: Mathematical and General 19, L441–L446.

Gillespie, D.T., 1976. A general method for numerically simulating the stochastic time evolution of coupled chemical reactions. Journal of Computational Physics 22, 403–434.

Green, M.A., 2007. Thin-film solar cells: review of materials, technologies and commercial status. Journal of Materials Science: Materials in Electronics 18, 15–19.

Hu, G., Huang, J., Orkoulas, G., Christofides, P.D., 2009a. Investigation of film surface roughness and porosity dependence on lattice size in a porous thin film deposition process. Physical Review E 80, 041122.

Hu, G., Orkoulas, G., Christofides, P.D., 2009b. Modeling and control of film porosity in thin film deposition. Chemical Engineering Science 64, 3668–3682.

Hu, G., Orkoulas, G., Christofides, P.D., 2009c. Regulation of film thickness, surface roughness and porosity in thin film growth using deposition rate. Chemical Engineering Science 48, 3903–3913.

Hu, G., Orkoulas, G., Christofides, P.D., 2009d. Stochastic modeling and simultaneous regulation of surface roughness and porosity in thin film deposition. Industrial & Engineering Chemistry Research 48, 6690–6700.

Huang, J., Hu, G., Orkoulas, G., Christofides, P.D., 2010. Dependence of film surface roughness and slope on surface migration and lattice size in thin film deposition processes. Chemical Engineering Science 65, 6101–6111.

Huang, J., Hu, G., Orkoulas, G., Christofides, P.D., 2011. Dynamics and lattice-size dependence of surface mean slope in thin film deposition. Industrial & Engineering Chemistry Research 50, 1219–1230.

Krč, J., Zeman, M., 2002. Experimental Investigation and Modelling of Light Scattering in a-Si:H Solar Cells Deposited on Glass/ZnO:Al Substrates 715. A.13.3.1–A.13.3.6.

Lauritsen, K.B., Cuerno, R., Makse, H.A., 1996. Noisy Kuramoto–Sivashinsky equation for an erosion model. Physical Review E 54, 3577–3580.

Leblanc, F., Perrin, J., 1994. Numerical modeling of the optical properties of hydrogenated amorphous-silicon-based p–i–n solar cells deposited on rough transparent conducting oxide substrates. Journal of Applied Physics 75, 1074.

Müller, J., Rech, B., Springer, J., Vanecek, M., 2004. TCO and light trapping in silicon thin film solar cells. Solar Energy 77, 917–930.

Ni, D., Christofides, P.D., 2005. Multivariable predictive control of thin film deposition using a stochastic PDE model. Industrial & Engineering Chemistry Research 44, 2416–2427.

Poruba, A., Fejfar, A., Remeš, Z., Špringer, J., Vaněček, M., Kočka, J., 2000. Optical absorption and light scattering in microcrystalline silicon thin films and solar cells. Journal of Applied Physics 88, 148–160.

Reese, J.S., Raimondeau, S., Vlachos, D.G., 2001. Monte Carlo algorithms for complex surface reaction mechanisms: efficiency and accuracy. Journal of Computational Physics 173, 302–321.

Rowlands, S.F., Livingstone, J., Lund, C.P., 2004. Optical modelling of thin film solar cells with textured interface using the effective medium approximation. Solar Energy 76, 301–307.

Springer, J., Poruba, A., 2004. Improved three-dimensional optical model for thin-film silicon solar cells. Journal of Applied Physics 96, 5329–5337.

Springer, J., Poruba, A., Vanecek, M., Fay, S., Feitknecht, L., Wyrsch, N., Meier, J., Shah, A., Repmann, T., Kluth, O., Stiebig, H., Rech, B., 2001. Proved optical model for thin film silicon solar cells. In: Proceedings of the 17th European Photovoltaic Solar Energy Conference, Munich, Germany.

Tao, G., Zeman, M., 1994. Optical modeling of a-Si:H based solar cells on textured substrates. In: 1994 IEEE First World Conference on Photovoltaic Energy Conversion. Conference Record of the Twenty Fourth IEEE Photovoltaic Specialists Conference – 1994 (Cat. No. 94CH3365-4), vol. 1, Waikoloa, HI, pp. 666.

van Sark, W., Brandsen, G.W., Fleuster, M., Hekkert, M.P., 2007. Analysis of the silicon market: will thin films profit? Energy Policy 35, 3121–3125.

Vlachos, D.G., Schmidt, L.D., Aris, R., 1993. Kinetics of faceting of crystals in growth, etching, and equilibrium. Physical Review B 47, 4896–4909.

Vorburger, T.V., Marx, E., Lettieri, T.R., 1993. Regimes of surface roughness measurable with light scattering. Applied Optics 32, 3401–3408.

Vvedensky, D.D., Zangwill, A., Luse, C.N., Wilby, M.R., 1993. Stochastic equations of motion for epitaxial growth. Physical Review E 48, 852–862.

Wächter, A., Biegler, L.T., 2006. On the implementation of an interior-point filter line-search algorithm for large-scale nonlinear programming. Mathematical Programming 106, 25–57.

Zeman, M., Vanswaaij, R., 2000. Optical modeling of a-Si:H solar cells with rough interfaces: effect of back contact and interface roughness. Journal of Applied Physics 88, 6436–6443.

Zhang, X., Hu, G., Orkoulas, G., Christofides, P.D., 2010a. Controller and estimator design for regulation of film thickness, surface roughness and porosity in a multiscale thin film growth process. Industrial & Engineering Chemistry Research 49, 7795–7806.

Zhang, X., Hu, G., Orkoulas, G., Christofides, P.D., 2010b. Multivariable model predictive control of thin film surface roughness and slope for light trapping optimization. Industrial & Engineering Chemistry Research 49, 10510–10516.

Zhang, X., Hu, G., Orkoulas, G., Christofides, P.D., 2010c. Predictive control of surface mean slope and roughness in a thin film deposition process. Chemical Engineering Science 65, 4720–4731.